

Concept Paper

# Removal of Iron from Pyrite-Rich Coal Refuse by Calcination and Magnetic Separation for Hydrometallurgical Extraction of Rare Earth Elements

Tushar Gupta<sup>1</sup>, Ahmad Nawab<sup>2</sup> and Rick Honaker<sup>2,\*</sup>

<sup>1</sup> MP Materials Mountain Pass Mine, 67750 Bailey Rd, Mountain Pass, CA 92366, USA

<sup>2</sup> Department of Mining Engineering, University of Kentucky, Lexington, KY 40506, USA

\* Correspondence: rick.honaker@uky.edu

**Abstract:** In the metallurgical extraction of rare earth elements (REEs), the ratio of contaminant ions to REEs in the leachate dictates the cost and operational efficiency of the downstream processes. The current study investigated the potential iron contamination removal from the feed to the hydrometallurgical process by calcination followed by magnetic separation. The 2.20 specific gravity sink fraction of Baker coal seam coarse refuse was pulverized to finer than 180  $\mu\text{m}$ , calcined at various temperatures, and separated into magnetic and non-magnetic fractions using a wet high-intensity magnetic separator at different field strengths. The untreated feed, calcined products, and their subsequent magnetic and non-magnetic fractions were subjected to acid leaching tests with 1.2 M sulfuric acid at 75 °C and 1% *w/v* solids concentration. The recovery of light and heavy rare earth elements (LREEs and HREEs, respectively) along with the concentration of common contaminant ions (Al, Ca, and Fe) were measured as output variables. The weight percent of magnetic material was maximized at approximately 29% by calcination at a temperature of 400 °C. Magnetic removal of this fraction using a field strength of 1.15 Tesla resulted in the rejection of 81% of the iron. Leaching of the magnetic fraction provided significantly higher Fe recovery relative to untreated feed material and the non-magnetic fraction. The non-magnetic fraction was subsequently calcined at 600 °C to dehydroxylate the clays and released the REE minerals in the same manner as the treatment of the original coarse refuse material. A comparison of the leachate elemental concentrations resulting from the leaching of both the calcined non-magnetic and original coarse refuse showed only a slight reduction in the iron content from the non-magnetic material. This finding combined with the REE loss in the magnetic fraction resulted in the conclusion that the magnetic removal step was unfavorable.

**Keywords:** calcination; magnetic separation; rare earth elements; leaching



**Citation:** Gupta, T.; Nawab, A.; Honaker, R. Removal of Iron from Pyrite-Rich Coal Refuse by Calcination and Magnetic Separation for Hydrometallurgical Extraction of Rare Earth Elements. *Minerals* **2023**, *13*, 327. <https://doi.org/10.3390/min13030327>

Academic Editor: Vysetti Balaram

Received: 26 January 2023

Revised: 19 February 2023

Accepted: 24 February 2023

Published: 26 February 2023



**Copyright:** © 2023 by the authors. Licensee MDPI, Basel, Switzerland. This article is an open access article distributed under the terms and conditions of the Creative Commons Attribution (CC BY) license (<https://creativecommons.org/licenses/by/4.0/>).

## 1. Introduction

Since the release of the U.S. Department of Energy Critical Mineral Strategy in 2011, coal sources have been extensively investigated as a potential resource for rare earth element (REE) extraction [1–3]. The REEs in all major U.S. coal deposits have been characterized, and efforts have been made to concentrate and/or extract REEs from coal-derived by-products, such as plant reject, fly ash, bottom ash, and acid mine drainage [4–6]. The conventional REE minerals are primarily concentrated by physical mineral processing techniques, such as gravity separation and froth flotation, and are subsequently extracted by hydrometallurgical processes [7–9]. However, the varied mineralogy and ultrafine particle size of the REEs associated with coal limit the use of standard physical separation unit operations [2,6]. Therefore, hydrometallurgical techniques, such as leaching, selective precipitation, and solvent extraction, are employed in combination for efficient REE extraction and purification [10–12].

Zhang, Honaker, and Yang et al. have extensively investigated the leaching behavior of raw coal from various locations using sulfuric, hydrochloric, and nitric acid. The

researchers reported that leaching of raw coal provides low (~10%–20%) REE recovery even after using high-strength acids (>1.0M) [13–15]. It was determined that the calcination of the coal-based feedstock effectively improved (~50%–70%) the leaching recoveries and reaction kinetics of the REEs [16–18]. The benefits are realized by converting the REEs to more soluble forms and/or by liberating the REE minerals encapsulated within the mineral matter, particularly clays. Yang also conducted a detailed investigation on the impact of leaching parameters on REE recovery [13]. It was determined that elevated temperatures (75 °C), lower solid-to-liquid ratio (1% S/L), higher acid strengths (>1.0M), and utilizing sulfuric acid/chloric acid favored high REE recovery. However, use of sulfuric acid in the leaching operation was preferred due to its lower cost and volatility of chloric acid at higher temperatures.

Interestingly, the high-temperature calcination pretreatment also increased the dissolution of contaminant ions, including aluminum, calcium, and iron, into the pregnant leach solution (PLS) due to the breakdown of crystal structure during clay dehydroxylation [19]. Elevated contaminant concentrations complicate the downstream processing of the PLS. For instance, a higher Fe (III) content relative to the REEs in the PLS decreases the extractant capacity for rare earth elements in solvent extraction [20]. During selective precipitation stages, Li et al. determined that elevated Fe concentrations cause REE adsorption onto the Fe-precipitate surfaces during Fe removal step [21]. Similarly, Nawab et al. studied the impact of Fe (III) concentration on oxalic acid precipitation of rare earth elements. It was concluded that the elevated Fe (III) content significantly increased the oxalic acid required to ensure high REE precipitation efficiency. Additionally, the presence of Fe (II) ions in the solution contaminated the rare earth oxalate product due to its precipitation as a ferrous oxalate [22].

Iron in coal is primarily associated with aluminosilicate clays and pyrites. Coal deposits with high pyrite content contain appreciable amounts of both massive and fine-grained pyrites which are primarily differentiated by the size of the mineralization [23]. While massive pyrite can be removed from the coal by washing, the framboidal pyrites, due to their small particle size, are not efficiently removed [24]. These pyrite framboids are responsible for iron contamination in the PLS and are a common host to trace elements, such as Pb, As, Cd, and REEs [24,25]. Because framboidal pyrite is fine-grained, and pyrites exhibit paramagnetic properties, traditional separation methods have very little applicability.

This work aims to characterize the pyrite present in coarse coal refuse from a bituminous coal source, which is a potential feedstock for REE extraction and has over 250 ppm of REEs. The objective of the work presented was to investigate the potential benefits resulting from enhancing the magnetic susceptibility of a pyrite-rich material by calcination and removal of iron-rich material by magnetic separation.

## 2. Materials and Methods

### 2.1. Materials

The source material for this project originated from the Baker (West Kentucky No. 13) coal seam located within the Illinois Coal Basin. A representative sample of coarse refuse generated at an operating coal preparation plant was collected in 18-kg increments every 30 min using a sweep-belt sampler over a three-hour operating period. The representative sample was subsequently density fractionated using a lab-scale float-sink system and a magnetite-based medium having a specific gravity (SG) of 2.20. The 2.20 SG sink fraction was wet screened to remove the entrained magnetite, air-dried, and finally pulverized to finer than 180 µm using a jaw crusher and a hammer mill (Figure 1). This material, which was observed to be rich in pyrite, was used as the feed source for calcination and acid leaching tests. Trace metal grade sulfuric acid was purchased from Thermo Scientific, Waltham, MA, USA, and was used to prepare 1.2M sulfuric acid solution by dilution with deionized water (ASTM D1193-06) for acid leaching tests.

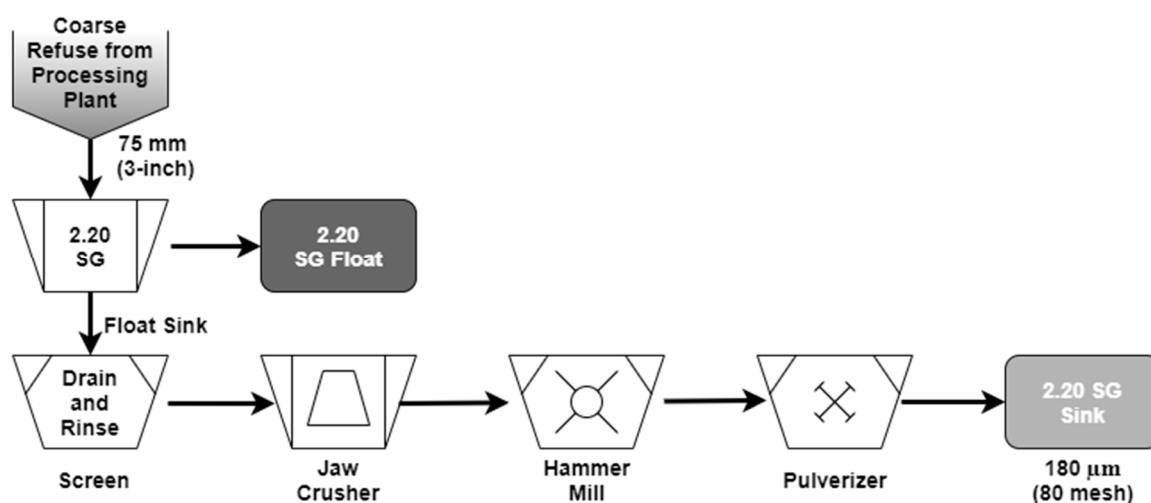


**Figure 1.** Process diagram of the sample preparation from the coarse refuse material collected from the processing plant treating Baker seam coal.

The 2.20 SG sink density fraction was predominantly composed of mineral matter with very low inherent moisture content. The 16% combustible content primarily originated from the pyritic sulfur and other sources along with carbonaceous shale. The total REE concentration was 288 ppm on a whole mass basis, of which approximately 85.72% were LREEs and 14.27% HREEs (Table 1). An X-ray diffraction (XRD) analysis was performed to characterize the sample mineralogy. Kaolinite  $[\text{Al}_2(\text{Si}_2\text{O}_5)(\text{OH})_4]$ , quartz  $[\text{SiO}_2]$ , and pyrite  $[\text{FeS}_2]$  were the three dominant minerals found in the sink fraction of the coarse refuse 2.2 SG sink sample (Figure 2). The XRF analysis for major and minor phases in the material is shown in (Table 2).

**Table 1.** Rare earth element concentration (whole mass basis, ppm) in 2.20 SG sink fraction of Baker coarse refuse material [Ash Content: 91.0%].

Sc	Y	La	Ce	Pr	Nd	Sm	Eu	Gd
18.39	24.13	48.44	97.25	12.74	48.09	10.80	1.98	8.87
Tb	Dy	Ho	Er	Tm	Yb	Lu	LREE	HREE
0.65	5.59	1.18	4.38	0.58	3.50	1.06	246.56	41.06

## 2.2. Methods

### 2.2.1. Calcination Tests

Calcination tests were carried out in a lab-scale Thermolyne F6020C-80 muffle furnace manufactured by Thermo Scientific, Waltham, MA, USA at different temperatures. The samples were heated at a constant rate of  $10\text{ }^\circ\text{C}/\text{min}$ , and the temperature was maintained inside the furnace for 2 h. A representative 30 g sample was evenly distributed into six crucibles (5 g/crucible). No chemical additives were added, and static atmospheric conditions were used. After completion of the test, the furnace was gradually cooled to room temperature. The calcined products were weighed and subjected to REE analyses and acid-leaching tests.

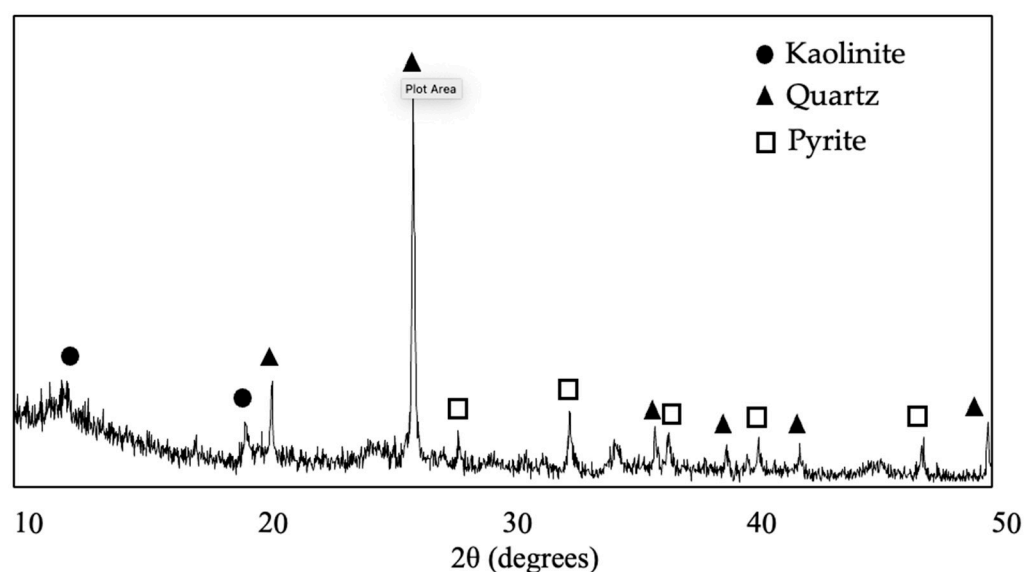


**Figure 2.** XRD analysis of the untreated 2.20 SG sink fraction of Baker seam coal (●-Kaolinite; ▲-Quartz; □-Pyrite).

**Table 2.** XRF analysis of major and minor phases (wt.%) for the 2.20 sink fraction of the Baker seam coal.

Sample	SiO <sub>2</sub>	Al <sub>2</sub> O <sub>3</sub>	Fe <sub>2</sub> O <sub>3</sub>	CaO	MgO	Na <sub>2</sub> O	K <sub>2</sub> O	P <sub>2</sub> O <sub>5</sub>	BaO	SrO	MnO
2.20 Sink	51.74	22.21	18.13	0.92	1.20	0.44	3.21	0.29	0.13	0.08	0.06

### 2.2.2. Magnetic Separation Tests

Magnetic separation tests were performed on the calcined products of the 2.20 SG sink fraction of the Baker coarse refuse. A slurry of 10% *w/v* was introduced into an L-4-20 wet high-intensity magnetic separator (WHIMS, L-4-20, Eriez, PA, USA) at various magnetic field strengths. The non-magnetic fraction of the feed slurry was collected into a bucket while feeding continuously. After all the feed was passed through the system, the magnetic field was turned off and the magnetic material was collected by washing with water. The magnetic and non-magnetic slurries were dewatered, air-dried, and subsequently split into subsamples for proximate and REE analyses. Magnetic separation tests using a field strength of 1.15 Tesla were performed on material that was calcined at temperatures of 400 °C, 500 °C, and 600 °C. The mass yield values to the magnetic and non-magnetic product streams were recorded. Additionally, tests were carried out on 2.20 SG sink material calcined at 400 °C at increasing magnetic field intensities from 2500 to 11,500 gauss.

### 2.2.3. Acid Leaching Tests

Acid leaching tests on the feed and calcined products were performed under a set of standard conditions in a three-neck round bottom flask with 1.2M sulfuric acid at 75 °C for 5 h at 1% *w/v* (10g/L) solid concentration. These conditions were used based on the findings from previous investigation [13]. The setup was equipped with condensers to minimize volumetric losses due to evaporation. For every test, a series of representative samples (15 mL) were collected at 10, 30, 60, 180, and 300 min from the start of the leaching process to establish leaching kinetics. Weights of the samples were recorded for mass balance evaluation. The samples were centrifuged at 4000 rpm for 10 min to collect the supernatants which were quickly filtered using a 0.45 µm PVDF membrane filter. The leaching tests were stopped at 300 min, and the residual slurry was filtered using a 5-µm pore-size filter paper. The filtrates were cooled to room temperature, and their volumes

were recorded. The filter cakes were dried in an oven at 60 °C for 12 h, and the solid residual dry weights were recorded.

Figure 3 depicts an overall process schematic after sample preparation involving roasting at different temperatures, magnetic separation at various magnetic field strengths followed by leaching operation at previously mentioned conditions. It should be noted that even though magnetic fraction collected from this process was a waste product, acid leaching experiments were still conducted to identify the leaching characteristics of rare earth elements and contaminants associated with the magnetic fractions.

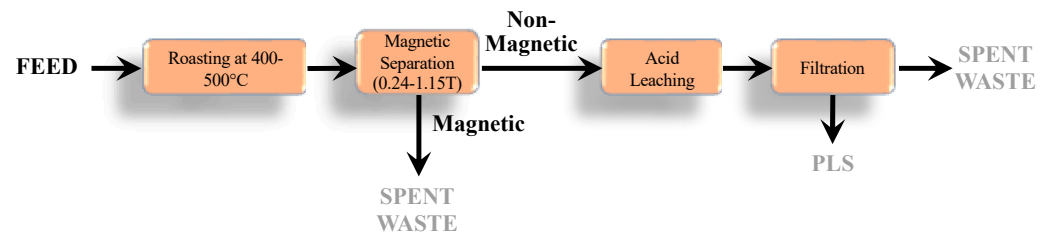


**Figure 3.** A general process diagram of the sample calcination, magnetic separation and acid leaching tested in this investigation.

#### 2.2.4. ICP-OES Analysis

Elemental analyses of feed material, pregnant leachate solution, and leaching solid residues were conducted using inductively coupled plasma optical emission spectrometry (ICP-OES, ARCOS, Spectro, Wilmington, MA, USA). The solid samples were digested by following the modified ASTM D6357-11 method. The process involved ashing a 1 g representative sample at 500 °C for 3 h followed by digesting 100 mg of the ashed sample in 20 mL Aqua Regia (HCl:HNO<sub>3</sub> = 3:1 *v/v*). Twenty mL of hydrofluoric acid was added to the tube, and the solution was evaporated at 150 °C. The solid residue obtained post evaporation was dissolved in 20 mL nitric acid and 30 mL deionized water. After this process, the solids were completely digested. After making up the desired volume using DI water, a 10 mL sample was collected for an ICP analysis. For PLS, a 10 mL representative sample was collected from bulk solution and analyzed using ICP.

REE recovery were calculated using the following expression, which is based on an elemental balance:

$$REE = 100 \times (C_1 \times V_1) / (C_s \times m_s + C_1 \times V_1) \quad (1)$$

where  $C_s$  and  $C_1$  represent REE concentrations (ppm) in the solid residual and final leachate;  $m_s$  (kg) weight of the leaching solid residue;  $V_1$  (liter) the volume of the final leachate. It must be noted that all REE contents in solids are based on a dry whole sample basis.

#### 2.2.5. Scanning Electron Microscope (SEM) Analysis

The feed and magnetic separation products were subjected to the SEM analysis to examine the surface texture, particle topography, and mineralogical composition using an FEI Quanta 250 Scanning Electron Microscope at the Electron Microscopy Center of the University of Kentucky (Lexington, KY, USA). The samples were mounted on a sample holder using electrically conductive double-sided carbon tape. Non-conducting samples were coated with platinum to a thickness of 7 nanometers to reduce beam penetration and allow for a sharper image. The elemental composition of the sample was determined by capturing the backscattered electrons and X-rays using a retractable energy-dispersive X-ray (EDX) detector.

### 3. Results and Discussions

#### 3.1. Pyrite Characterization

A wide variety of pyrite forms were found in the SEM analysis of the untreated 2.20 SG sink material collected from the Baker seam coal coarse refuse. The sample contained regular framboidal pyrites with pyrite microcrystals ranging from 100 nm to 1 µm,

as well as massive pyrites ranging from 10–50  $\mu\text{m}$ . Additionally, irregular pyrite aggregates were determined to be associated with quartz and clay minerals as large compound particles (Figure 4). All pyrite crystals in the feed were found to be angular and with no observable porosity.

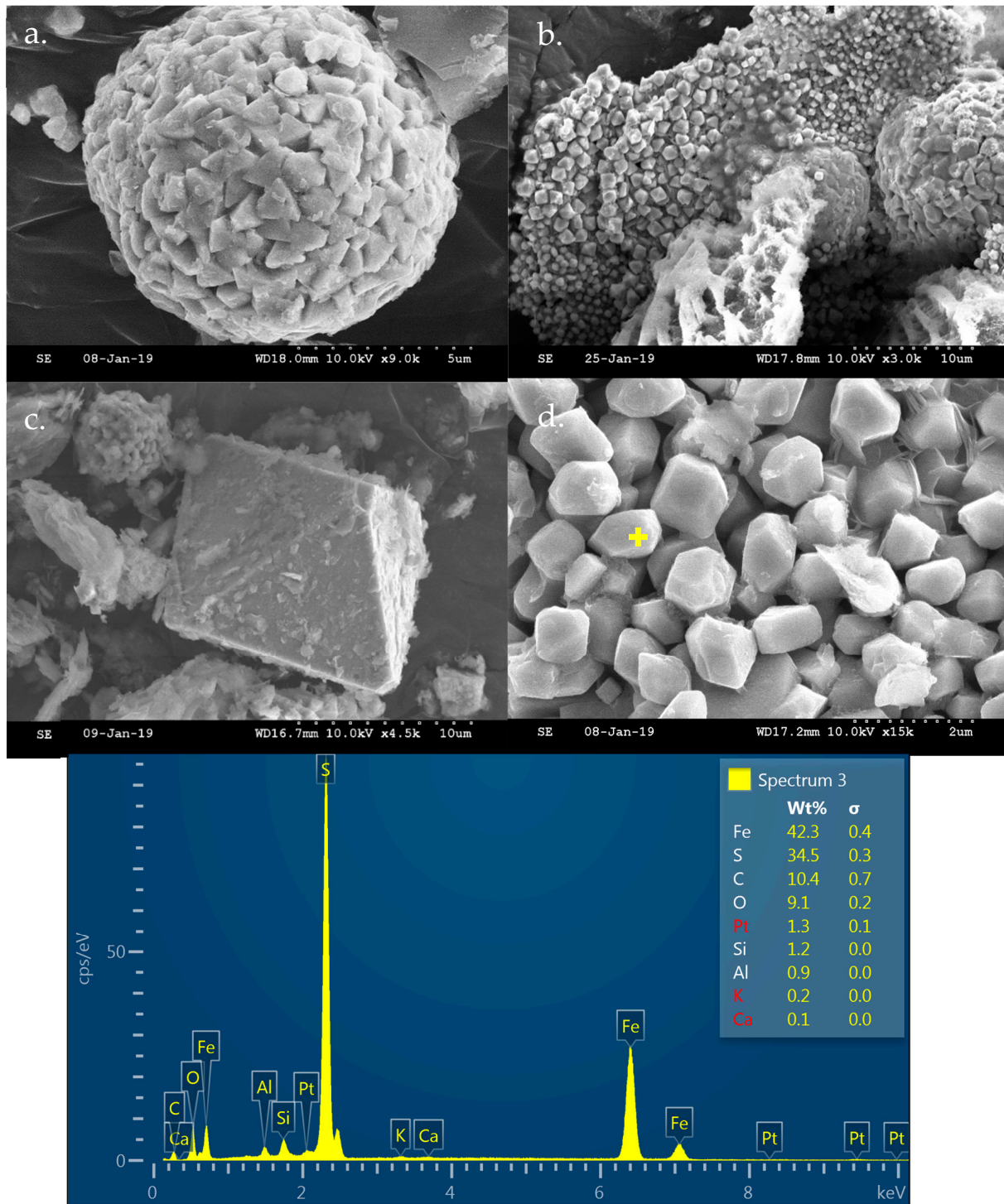


**Figure 4.** SEM images of various pyrite types found in the 2.20 SG sink fraction of the Baker seam coal course refuse material and EDX analysis showing the overall composition of these particles: (a) regular spherical shaped clusters, (b) composite mineral agglomerates, (c) large hexagonal crystals, and (d) small grain crystal clumps.

The total sulfur content of 9.7% in the 2.20 SG sink fraction primarily originated from pyrite. The sample was calcined at temperatures ranging from 100–1000 °C, and the calcined products were subjected to a dry magnetic separation using a handheld neodymium magnet. The calcination products between the temperatures of 400–600 °C showed magnetic susceptibility, while the calcinated material at all other temperatures was not affected by the application of an external magnetic field.

### 3.2. Magnetic Separation

Subsequently, wet high-intensity magnetic separation tests were performed at the peak magnetic field intensity of 11,500 gauss (1.15 Tesla). The magnetic and non-magnetic fractions were collected, dewatered, and air-dried. The magnetic and non-magnetic products were weighed and subjected to XRD, SEM, and REE analyses to determine the mineralogy and partitioning of REEs. The mass yield for the magnetic separation tests of the calcination products at different temperatures is provided in Figure 5. The magnetic mass yield was maximum at 400 °C and decreased with an increase in calcination temperature. Iron grades in the magnetic products calcined at 400 °C, 500 °C, and 600 °C were 38.9%, 39.3%, and 56.5%, respectively, whereas corresponding non-magnetic products had Fe grades of 3.7%, 10.4%, and 13.15%, respectively. As discussed later in this manuscript, the differences in the iron grades appear to be primarily due to the entrapment of non-magnetic products when the mass yield to the magnetic fraction is the highest. Figure 6 shows the magnetic and non-magnetic fractions of the calcined products at 400 °C and 500 °C collected by magnetic separation.

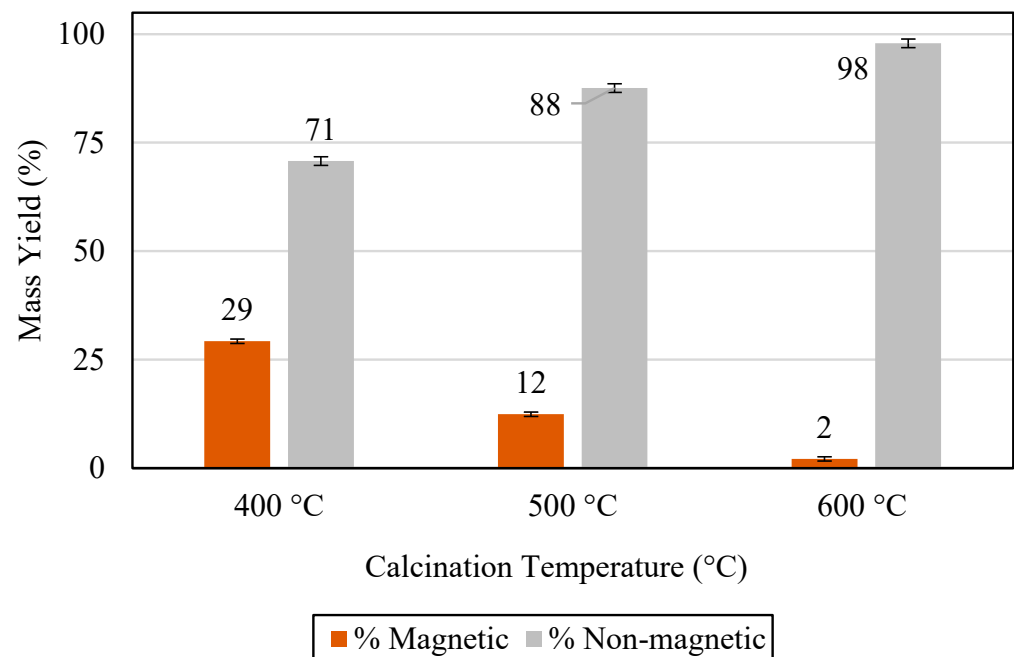


**Figure 5.** The mass yield obtained from magnetic separation tests on calcined products of the 2.20 SG sink fraction of Baker seam coal generated at three temperatures under a field strength of 11,500 Gauss.

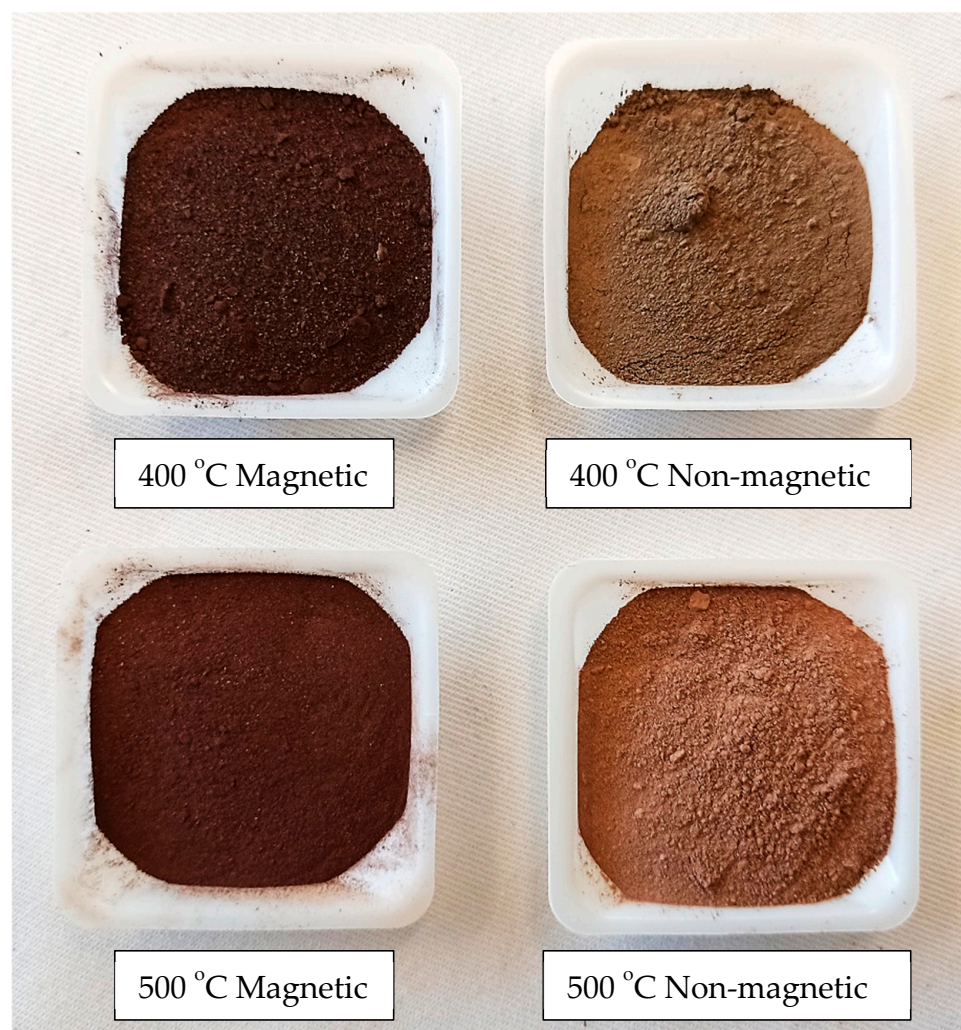


**Figure 6.** The collected magnetic and non-magnetic fractions obtained from the magnetic separation of Baker seam coal 2.20 SG sink fraction calcined at 400 °C and 500 °C.

The XRD analysis of the magnetic fraction was performed to ascertain the phase changes in mineralogy because of calcination at 400 °C and 500 °C (Figure 7). The major minerals found in the magnetic fractions were quartz [ $\text{SiO}_2$ ], kaolinite [ $\text{Al}_2(\text{Si}_2\text{O}_5)(\text{OH})_4$ ], and hematite [ $\text{Fe}_2\text{O}_3$ ]. As compared to the feed, the pyrite in the sample was transformed to hematite during the high-temperature calcination process in the presence of oxygen. Most of the iron-rich pyrite was converted to magnetic hematite and reported to the magnetic fraction. Moreover, the oxidation of pyrite aggregates associated with the compound particles in the feed resulted in the entrapment of quartz and kaolinite in the magnetic fraction due to incomplete liberation, resulting in a lower Fe grade. This observation is supported by the mass distribution percent data of other contaminants and REEs reported later in the investigation. Contrarily, a higher Fe grade at 600 °C is likely due to the extraction of purely magnetic particles. It has been found previously that the change in the magnetic behavior of pyrite during thermal decomposition and oxidation is very complex and depends on factors such as temperature, oxygen concentration, and particle size [26,27].

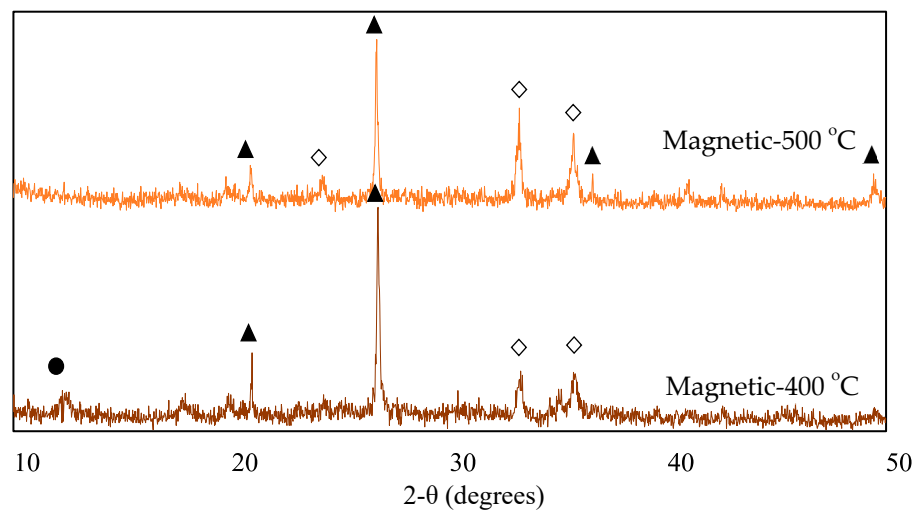


**Figure 7.** XRD analysis of the magnetic fraction of the 2.20 SG sink fraction of Baker seam coal calcined at 400 °C and 500 °C (●-Kaolinite; ▲-Quartz; ◇-Hematite).

Since the magnetic fraction mass yield was highest from the 400 °C calcined product (Figure 5), magnetic separation tests were carried out on the 400 °C treated material at varying magnetic field strengths. A 12% magnetic mass yield occurred using a field strength of 2400 gauss, suggesting that the iron oxide has higher sensitivity to an external magnetic field than the parent pyrite which has a weak response to a magnetic field. The magnetic fraction yield increased with an elevation in magnetic field strength suggesting that the pyrite crystals intermixed and interbedded with other mineral forms also reported to the magnetic stream when a sufficiently high magnetic field was applied (Figure 8).

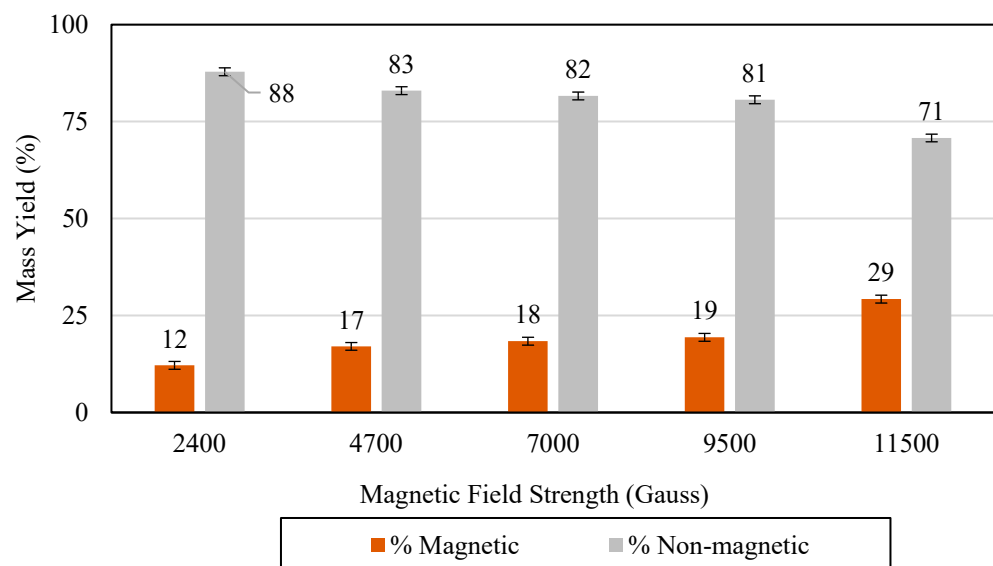


**Figure 8.** Mass yield of magnetic separation tests at varying magnetic field intensities for the 2.20 SG sink fraction of Baker seam coal calcined at 400 °C.

Increasing the magnetic field strength also improved Fe removal from the feed (Table 3). At 2400 Gauss, 53% of the Fe in the 400 °C calcined feed reported to the magnetic fraction which increased to approximately 81% at 11,500 Gauss. Thermal treatment of the material at 500 °C significantly reduced the Fe removal, with only 35% Fe removed at 11,500 gauss. Since most of the Fe reported to the magnetic portion at higher field strengths, adding a magnetic separation step is expected to decrease the base consumption in the downstream processes. Additionally, ICP-OES analyses revealed that the non-magnetic

fraction contained higher concentrations of both light and heavy REEs (Figure 9). Therefore, magnetic separation of calcinated material can be viably used as a physical separation method for enriching REEs in the feed to the hydrometallurgical circuit. The REE contents in the non-magnetic fraction of 2.20 SG sink calcined at 400 °C increased by 15% as compared to the untreated feed. As most of the pyrite was converted to a magnetic oxide and removed by magnetic separation, the higher REE concentrations could be associated with other mineral forms in the feed, possibly clays. Similar explanations of the association of REEs with kaolinite and illite minerals have been postulated by Moldoveanu and Papangelakis, Valian, and Zhang et al. [28–30].

**Table 3.** Mass distribution % in magnetic and non-magnetic products obtained at different magnetic strengths for 400 °C and 500 °C calcined material.

Temperature	Gauss	Fraction	LREEs	HREEs	Al	Ca	Fe
400 °C	2400	Mag	6.8	10.1	5.2	10.3	56.4
		Non-Mag	93.2	89.9	94.8	89.7	43.6
	4700	Mag	11.0	14.2	8.6	19.9	71.0
		Non-Mag	89.0	85.8	91.4	80.1	29.0
	7000	Mag	13.2	16.0	10.1	20.9	72.5
		Non-Mag	86.8	84.0	89.9	79.1	27.5
	9500	Mag	13.6	16.1	10.3	24.6	76.7
		Non-Mag	86.4	83.9	89.7	75.4	23.3
	11,500	Mag	23.4	25.4	19.1	40.4	81.3
		Non-Mag	76.6	74.6	80.9	59.6	18.7
500 °C	2400	Mag	2.0	3.0	1.5	2.1	17.2
		Non-Mag	98.0	97.0	98.5	97.9	82.8
	4700	Mag	3.1	4.4	2.4	5.5	23.2
		Non-Mag	96.9	95.6	97.6	94.5	76.8
	7000	Mag	4.9	6.3	3.7	6.8	31.1
		Non-Mag	95.1	93.7	96.3	93.2	68.9
	9500	Mag	6.1	7.7	4.9	13.2	35.8
		Non-Mag	93.9	92.3	95.1	86.8	64.2
	11500	Mag	8.8	9.2	6.5	13.0	34.8
		Non-Mag	91.2	90.8	93.5	87.0	65.2

### 3.3. Leaching Experiments

Leaching tests were carried out on the magnetic and non-magnetic fractions of calcination products separated at 11,500 gauss with 1.2M sulfuric acid at 75 °C and 1% *w/v* solid concentration. Baseline values were established by leaching the untreated sample under the same leaching conditions. Additionally, calcination products of 400 °C, 500 °C, and 600 °C were subjected to acid leaching for comparison purposes. The recovery of LREEs and HREEs along with the concentration of Al, Ca, and Fe in the PLS was measured as the response. For a sample calcined at 400 °C, the LREE and HREE recoveries were approximately 51 and 11 absolute percentage points lower than those calcined at 600 °C, respectively (Figure 10). The bulk of this difference in LREE recovery resulted from the variation in the recovery of lanthanum, cerium, and neodymium, which typically are the bulk of the elements comprising the LREEs. The concentration of Al in the PLS was higher at 600 °C, suggesting that the aluminosilicates were transformed to a more soluble form at 600 °C [11]. The increase in the leachability of Fe at 400 °C as compared to the untreated material and the subsequent decrease at 600 °C suggests that the pyrite was oxidized to a more stable oxide at 600 °C which is harder to leach as compared to the more leachable form at 400 °C. The calcium concentration in the PLS was the same at the two calcination

temperatures. Decomposition of calcium carbonate occurs in 700–800 °C temperature range, and thus calcination at 400–600 °C did not alter the mineralogy of calcite [31]. Overall, calcination of the feed at 600 °C followed by acid leaching had better REE leaching results than the sample calcined at 400 °C.

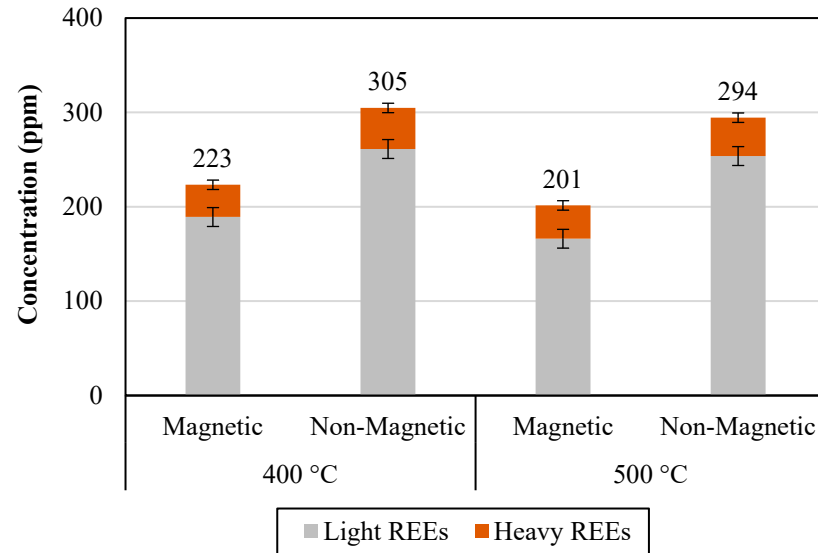


**Figure 9.** REEs concentration (ppm) in the magnetic and non-magnetic fractions of the 2.20 SG sink of Baker seam coal calcined at 400 °C and 500 °C (Magnetic Field: 1.15 Tesla).

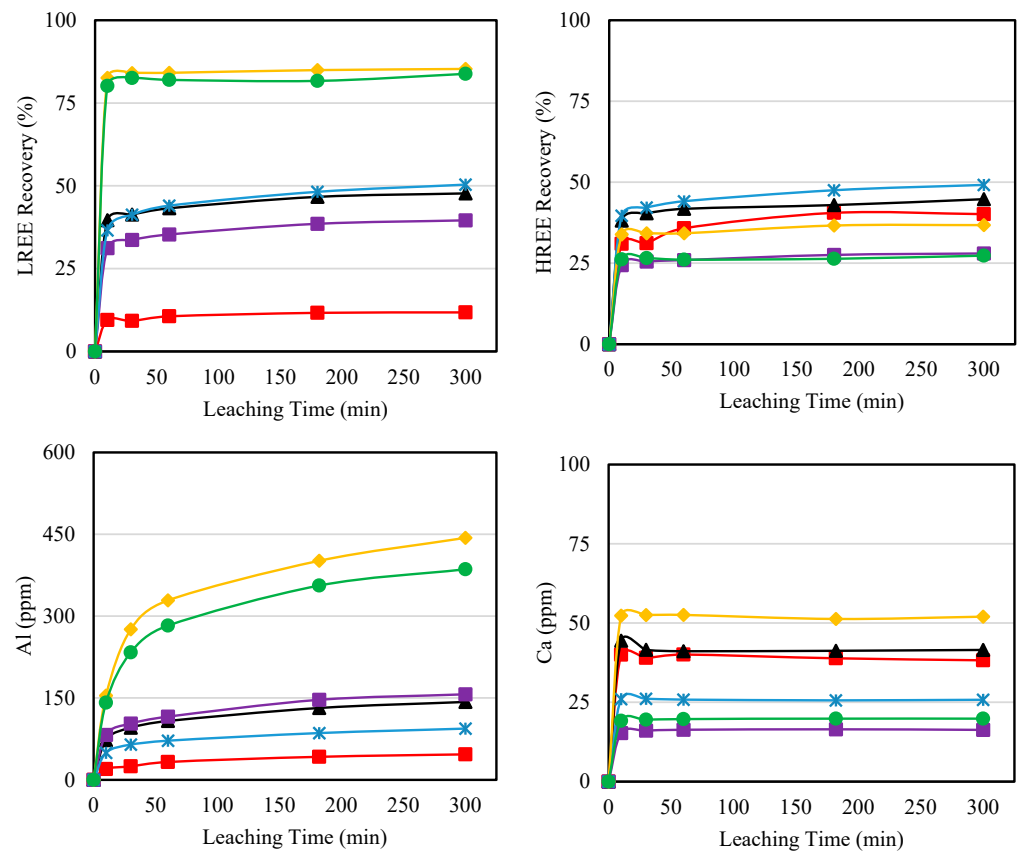


**Figure 10.** Cont.

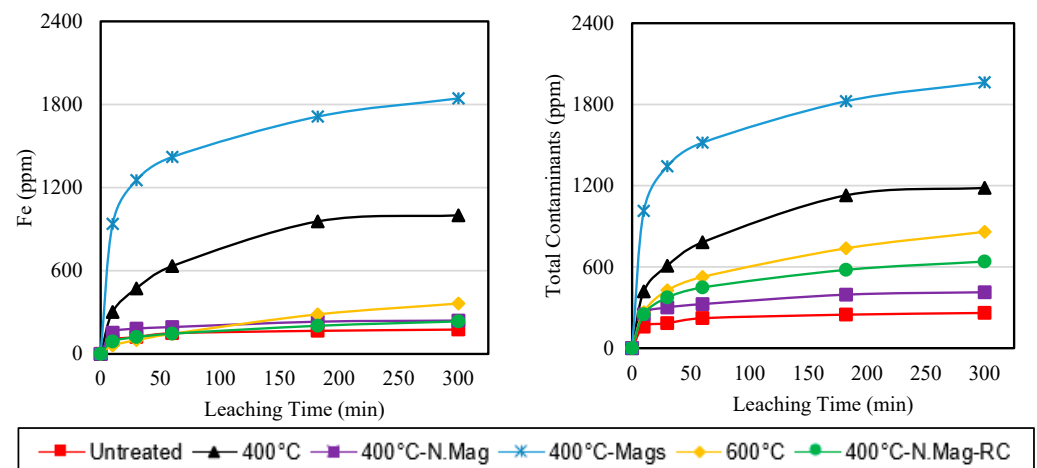


**Figure 10.** Acid leaching test results with 1.2M H<sub>2</sub>SO<sub>4</sub> for the 2.20 SG sink calcined products at different temperatures. (Mags = Magnetic; N. Mag = Non-magnetic; N. Mag-RC = Non-magnetic fraction re-calcined at 600 °C).

When the calcination products at 400 °C were separated into the magnetic and non-magnetic fractions and leached separately, the hematite-rich magnetic fraction (400 °C-Mags) showed higher HREE leaching recoveries as compared to the 600 °C calcined material (600 °C). However, the concentration of Al and Ca was considerably lower, while the Fe concentration was elevated by more than 450%. This suggested that the magnetic fraction had easy-to-leach HREEs associated with the hematite. The 400 °C non-magnetic material (400 °C-N. Mag) had a 50% lower concentration of contaminants in the PLS relative to the 600 °C calcined material. However, the REE recovery from 400 °C non-magnetic fraction also dropped by ~50% absolute points. When the 400 °C non-magnetic material was re-calcined at 600 °C (400 °C-N. Mag-RC), the recovery of LREEs was found to increase and was similar to the calcination products of feed at 600 °C. Additionally, with the removal of most of the pyrites as iron oxides in the magnetic fraction, the increase in the LREE recovery possibly originated from the REEs associated with clays. This hypothesis is supported by the identical Al concentration trends achieved for the 400 °C tailings fraction re-calcined at 600 °C and the 2.20 SG sink feed calcined at 600 °C. The lower HREE recoveries, however, were partly due to the loss of highly leachable HREEs to the magnetic fraction.

Interestingly, even though most of the Fe was removed to the magnetic fraction, the Fe content in the leachate solution of non-magnetic (400 °C-N. Mag) and re-calcined material (400 °C-N. Mag-RC) was fairly close to the 600 °C roasted material PLS. This was due to a significant change in the Fe recoveries. The non-magnetic fraction, re-calcined non-magnetic fraction, and 600 °C had 75%, 68%, and 35% Fe recoveries, respectively. It was postulated that the non-magnetic material contained soluble iron-bearing minerals, therefore, Fe recovery remained high even after re-calcining the material. Comparatively, most of the iron in the original 600 °C calcined material converted to a chemically inert form, and primarily soluble iron-bearing minerals were leached, resulting in lower Fe recovery.

On the other hand, the LREE recovery for the samples calcined at 500 °C and 600 °C were found to be similar (Figure 11). No benefits of calcination at the two temperatures were observed for the HREE recovery compared to the untreated feed. The calcination products had similar Ca leaching characteristics for both temperature values, whereas the Al concentration for 600 °C calcined material was relatively higher. Comparatively, the Fe content was higher for 500 °C than 600 °C, suggesting a more leachable form of iron oxide at 500 °C which, when subjected to a higher temperature, was transformed to more stable mineralogy. When the magnetic separation products from 500 °C calcination were leached, significant dissolution of Fe was observed for the magnetic fraction (500 °C-Mags), suggesting that the phase transformation of pyrite to hematite also improved the leaching characteristics of Fe. Higher HREE recoveries were observed for the HREEs associated

with the magnetic fraction as compared to all other samples. This finding suggests that some HREEs were associated with the pyrite and were converted to more leachable forms when calcined at 500 °C. The non-magnetic fraction (500 °C-N. Mag) of the 500 °C had similar total contaminants to those of the 600 °C and showed similar leaching characteristics concerning the REEs. The above observations suggest that calcination at 500 °C followed by magnetic separation and leaching had no significant benefit over the calcination at 600 °C.

To summarize, the magnetic separation provides promising means for effective Fe removal and REE content upgradation in the solid feed to the leaching operation. However, the leaching recovery from the non-magnetic fraction was significantly lower than the 600 °C calcined material. Even though re-roasting the non-magnetic fraction at 600 °C elevated the rare earth element recovery, the total contaminant concentration was close to the directly calcined material. The lower rare earth element leaching recovery from 400 °C calcined non-magnetic fraction coupled with the additional magnetic separation cost would likely make the economics less favorable compared to simple 600 °C thermal treatment. Hence, the proposed process is advantageous only if high REE recovery can be realized from the non-magnetic fraction or if there is a substantial increase in the REE valuation in the future.

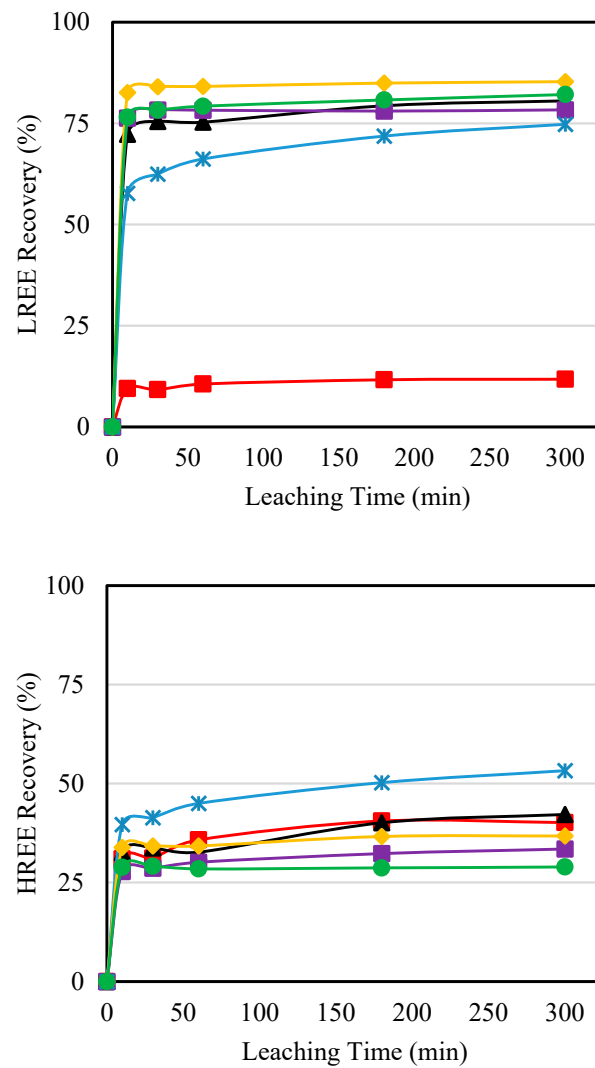


Figure 11. Cont.

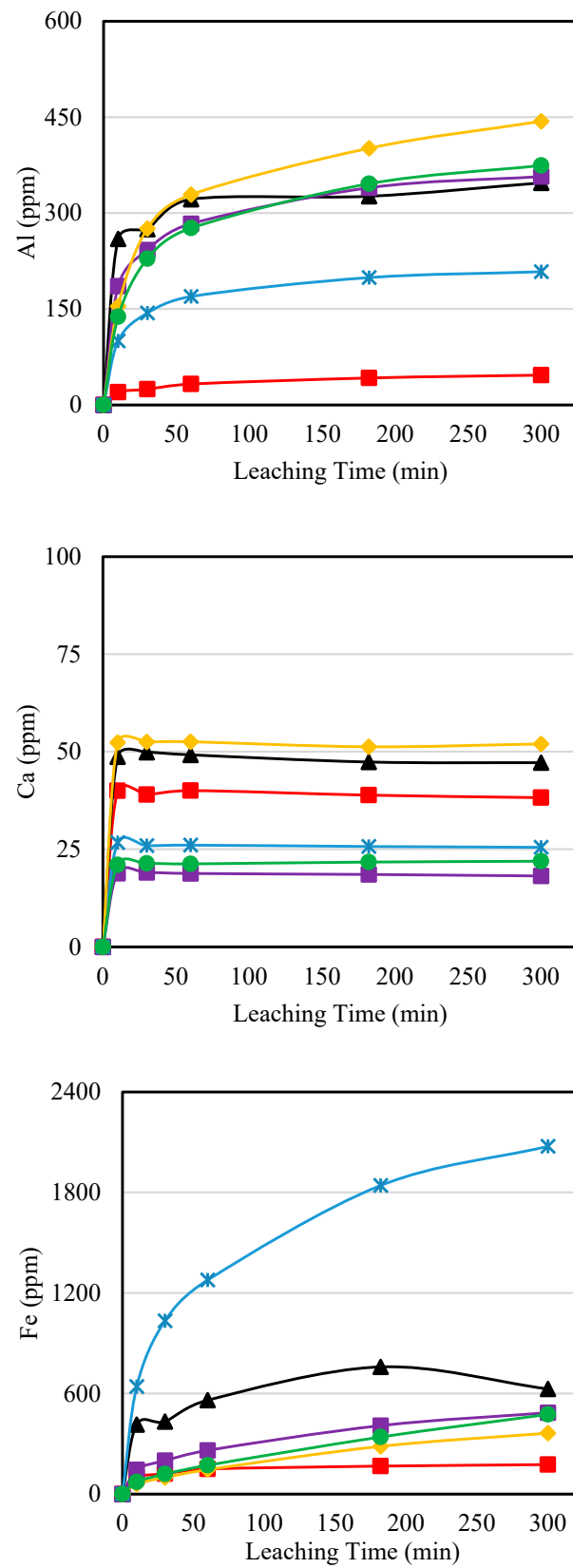
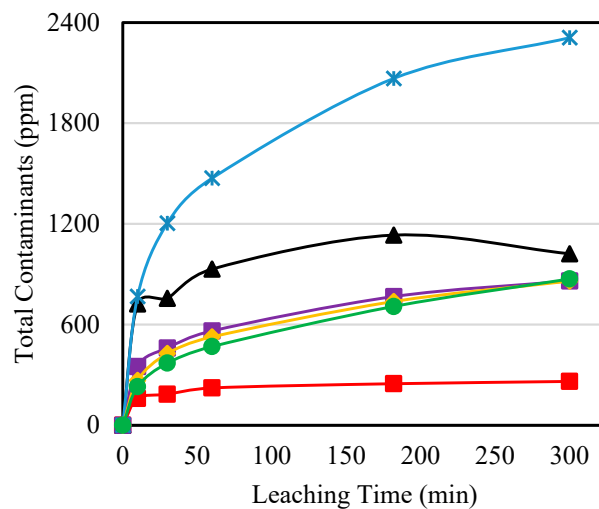


Figure 11. Cont.



—■— Untreated —▲— 500°C —■— 500°C-N.Mag —\*— 500°C-Mags —◆— 600°C —●— 500°C-N.Mag-RC

**Figure 11.** Acid leaching test results with 1.2M H<sub>2</sub>SO<sub>4</sub> for the 2.20 SG sink calcined products at different temperatures. (Mags = Magnetic; N. Mag = Non-magnetic; N. Mag-RC = Non-magnetic fraction re-calcined at 600 °C).

### 3.4. SEM Characterization:

In the acid leaching tests, the magnetic fraction for the samples calcined at 400 °C and 500 °C was found to have better leaching characteristics based on higher HREE recovery values and lower concentrations of Al and Ca. The increase in the HREE recoveries correlated well with an increase in Fe concentration in the pregnant leach solution (PLS). The initial decomposition of the pyrite particles resulted in the formation of iron oxide identified as hematite by the XRD analysis of the magnetic fractions (Figure 7). However, based on the physical evidence provided by the SEM analysis of the magnetic fractions, it appeared that at lower temperatures, pyrite microcrystals oxidized and were converted to porous iron oxide clusters with no melting and little dimensional change (Figure 12). However, data is not available to definitively prove this observation. Energy dispersive X-ray (EDX) analyses of the calcined pyrite suggested a Fe/O ratio closer to hematite. The increased porosity of the hematite layer is suggestive of a significant mass transfer by sulfur evolution through the pores of the particle as SO<sub>2</sub>. When the internal pressure exceeds the cohesion stress of the hematite rim, the particles cleave, leading to fissures. Evidence shows completely decomposed pyrite particles exhibiting massive fissures, which supports this hypothesis (Figure 12). Opening of these channels within the particle assists in the dissolution of associated HREEs, as observed in the acid leaching tests.

### 3.5. Flowsheet Development

An analysis of the leaching data suggested that acid leaching of the calcination products performed at 400 °C led to a 50% reduction in contaminants relative to 600 °C by using simple magnetic separation. While the overall gangue contamination reduced in the process, it was unfortunately accompanied by lower concentrations of REEs in the leach solution. As such, it was concluded that magnetic removal does not provide promising means for effective REE extraction. However, if this process is considered, REE recovery and purification processes are expected to follow Figure 13. This process flow was inspired by the flowsheet for REE extraction developed previously by the University of Kentucky [14,29,32].

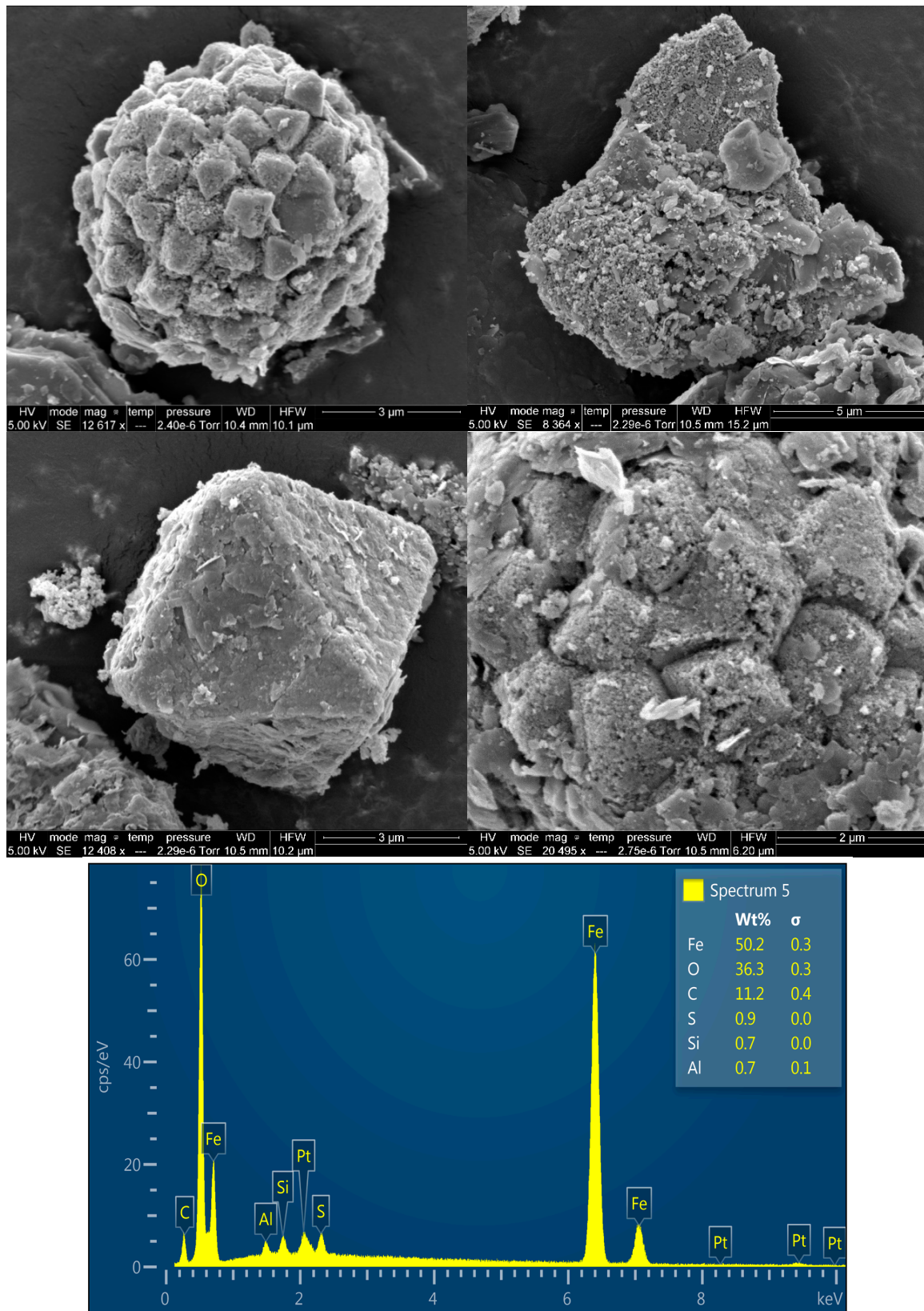
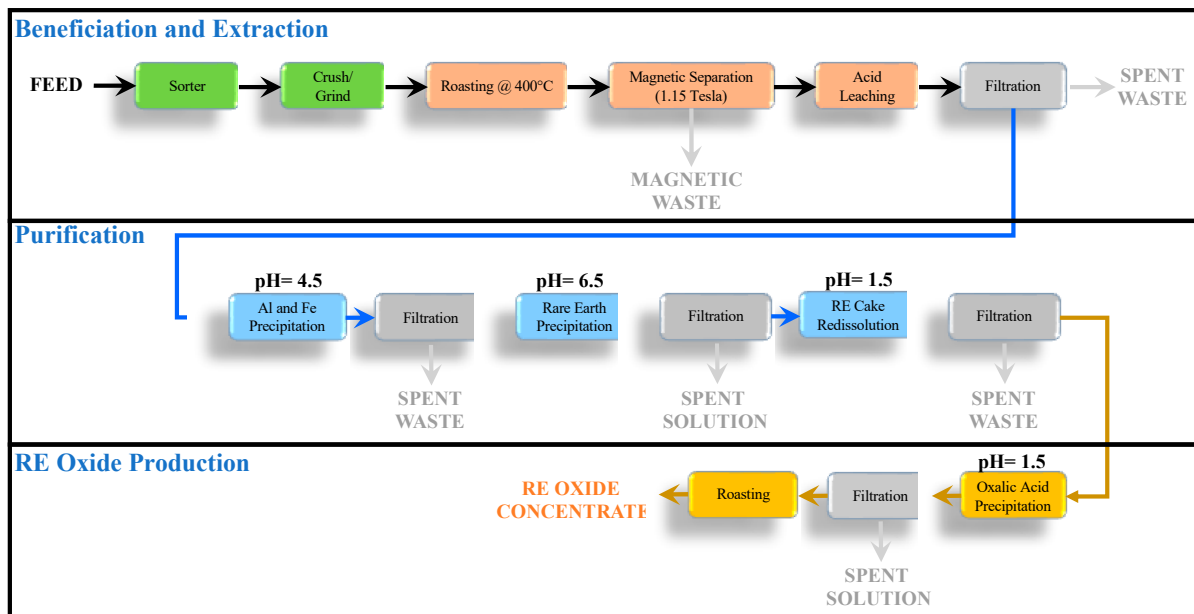


Figure 12. SEM analysis of the 2.20 SG sink fraction of Baker seam coal calcined at 400 °C and EDX analysis suggesting the formation of iron oxide and the crystal structure of pyrite being intact.



**Figure 13.** Flowsheet for single-stage calcination followed by magnetic separation in the hydrometallurgical extraction and purification of REEs from coal-based feedstocks.

REE recovery process can be subdivided into three stages: (1) Beneficiation and Extraction, (2) Purification, and (3) RE Oxide production. In the first stage, the crushing process reduces the run-of-mine material to a top particle size of 50 mm, which is subsequently sorted by an X-ray sorter to reject the lower-density fractions. The X-ray sorted product is reduced to a top particle size of 180  $\mu\text{m}$ , which is suitable for calcination and magnetic separation. The calcination process liberates the REEs by thermal treatment in the presence of air. The oxidized product is then split into magnetic and non-magnetic fractions by magnetic separation at 400  $^{\circ}\text{C}$ , and the non-magnetic fraction is dissolved in solution by acid leaching. In the second stage, major contaminants in the solution will be removed by raising the solution pH to 4.5 using NaOH, and the filtrate will be used for REE precipitation at pH 6.5. Contaminant removal prior to REE precipitation is crucial to maximizing REE purity in the oxalic acid precipitation stage [19]. RE enriched cake will then be subjected to redissolution using HCl to solubilize REEs [32]. In the final stage, rare earth elements will be precipitated using oxalic acid precipitant due to its selectivity towards rare earth elements [22]. Considering the versatility of this flowsheet, it can be applied to any other process as well to remove the contaminants and obtain a high-purity RE oxide product.

#### 4. Conclusions

Magnetic separation tests were performed on the 2.20 SG sink fraction of the Baker seam coal coarse waste calcined at 400  $^{\circ}\text{C}$ , 500  $^{\circ}\text{C}$ , and 600  $^{\circ}\text{C}$ . It was determined that magnetic mass yield was highest from 400  $^{\circ}\text{C}$  material at 11,500 gauss field strength and dropped with an increase in the calcining temperature, suggesting phase transformation to a more stable hematite with lower dissolution characteristics. Metallurgical accounting around the magnetic separator revealed that approximately 80% of the Fe was removed from the feed at 11,500 gauss field strength. Following the iron removal, acid leaching tests under standardized conditions using 1.2 M sulfuric acid were performed on the magnetic and non-magnetic fractions of both 400  $^{\circ}\text{C}$  and 500  $^{\circ}\text{C}$  calcined material to assess the difference in the leaching characteristics of REEs and common gangue minerals. It was found that the non-magnetic portion of the calcined pyrite-rich material contained higher concentrations of REEs than the magnetic fraction. The total contaminant concentration in the PLS was significantly lower in the non-magnetic fraction of 400  $^{\circ}\text{C}$  calcined material than in raw 400  $^{\circ}\text{C}$  and 600  $^{\circ}\text{C}$  roasted solids. However, light and heavy rare earth element

leaching recoveries dropped by approximately 51 and 10 absolute percentage points. Since REE liberation from clays is essential for their efficient leaching, lower recoveries likely resulted due to the stable nature of kaolinite at 400 °C. The inability to obtain elevated REE recoveries from the non-magnetic fraction was deduced to make the process more cost exhaustive compared to direct roasting. The mechanism of phase transformation of pyrites was established using XRD and SEM analyses to support the observations in the acid leaching tests. At lower temperatures, pyrites were decomposed to hematite, and SO<sub>2</sub> was released. The hematite formed as a product reported to the magnetic fraction by application of an external magnetic field. This hematite was found to have higher visible porosity which would facilitate the dissolution of associated trace elements. Additionally, a fraction of the total HREEs were found to be associated with pyrites which had different leaching characteristics as compared to the residual HREEs in the non-magnetic fraction. Based on the findings of the study, a flowsheet for further processing of the PLS with optimum process setpoints was provided. It is anticipated that selective precipitation of contaminants followed by REE precipitation will provide an enriched REE cake for further processing. Finally, oxalic acid precipitation can be employed for the generation of high-purity REE oxide cake from upgraded leach solution.

**Author Contributions:** T.G.: Conceptualization, Methodology, Formal analysis, Investigation, Writing—original draft, Writing—review and editing. A.N.: Conceptualization, Methodology, Data curation, Formal analysis, Writing—review and editing. R.H.: Conceptualization, Writing—review and editing, Supervision, Project administration, Funding acquisition. All authors have read and agreed to the published version of the manuscript.

**Funding:** This material is based upon work supported by the Department of Energy Award Number DE-FE0031827.

**Data Availability Statement:** The data presented in this study are available on request from the corresponding author.

**Conflicts of Interest:** The authors declare no conflict of interest.

## References

1. Seredin, V.V.; Dai, S.; Sun, Y.; Chekryzhov, I.Y. Coal deposits as promising sources of rare metals for alternative power and energy-efficient technologies. *Appl. Geochem.* **2013**, *31*, 1–11. [[CrossRef](#)]
2. Zhang, W.; Rezaee, M.; Bhagavatula, A.; Li, Y.; Groppo, J.; Honaker, R. A review of the occurrence and promising recovery methods of rare earth elements from coal and coal by-products. *Int. J. Coal Prep. Util.* **2015**, *35*, 295–330. [[CrossRef](#)]
3. Honaker, R.; Groppo, J.; Bhagavatula, A.; Rezaee, M.; Zhang, W. Recovery of rare earth minerals and elements from coal and coal byproducts. In Proceedings of the International Coal Preparation Conference 2016, Louisville, Kentucky, 20 April 2016; pp. 25–27.
4. Fu, B.; Hower, J.C.; Zhang, W.; Luo, G.; Hu, H.; Yao, H. A review of rare earth elements and yttrium in coal ash: Content, modes of occurrences, combustion behavior, and extraction methods. *Prog. Energy Combust. Sci.* **2022**, *88*, 100954. [[CrossRef](#)]
5. Luttrell, G.H.; Kiser, M.J.; Yoon, R.-H.; Noble, A.; Rezaee, M.; Bhagavatula, A.; Honaker, R.Q. A Field Survey of Rare Earth Element Concentrations in Process Streams Produced by Coal Preparation Plants in the Eastern USA. *Min. Metall. Explor.* **2019**, *36*, 889–902. [[CrossRef](#)]
6. Gupta, T.; Ghosh, T.; Akdogan, G.; Bandopadhyay, S. Maximizing REE Enrichment by Froth Flotation of Alaskan Coal Using Box-Behnken Design. *Min. Metall. Explor.* **2019**, *36*, 571–578. [[CrossRef](#)]
7. Krishnamurthy, N.; Gupta, C.K. *Extractive Metallurgy of Rare Earths*; CRC press: Boca Raton, FL, USA, 2004.
8. Wang, M.H.; Zeng, M.; Wang, L.S.; Zhou, J.H.; Cui, D.L.; Wang, Q.; Weng, R.; Chen, X. Catalytic leaching process of bastnaesite with hydrochloric acid after oxidation roasting pretreatment. *J. Chin. Soc. Rare Earths* **2013**, *31*, 148.
9. Feng, X.-L.; Long, Z.-Q.; Cui, D.-L.; Wang, L.-S.; Huang, X.-W.; Zhang, G.-C. Kinetics of rare earth leaching from roasted ore of bastnaesite with sulfuric acid. *Trans. Nonferrous Met. Soc. China* **2013**, *23*, 849–854. [[CrossRef](#)]
10. Peelman, S.; Kooijman, D.; Sietsma, J.; Yang, Y. Hydrometallurgical Recovery of Rare Earth Elements from Mine Tailings and WEEE. *J. Sustain. Metall.* **2018**, *4*, 367–377. [[CrossRef](#)]
11. Nawab, A.; Yang, X.; Honaker, R. An acid baking approach to enhance heavy rare earth recovery from bituminous coal-based sources. *Miner. Eng.* **2022**, *184*, 107610. [[CrossRef](#)]
12. Zhang, W.; Honaker, R.; Groppo, J. Concentration of rare earth minerals from coal by froth flotation. *Miner. Metall. Process.* **2017**, *34*, 132–137. [[CrossRef](#)]
13. Yang, X. Leaching Characteristics of Rare Earth Elements from Bituminous Coal-Based Sources. Ph.D. Thesis, University of Kentucky, Lexington, KY, USA, 2019. Available online: <https://orcid.org/0000-0002-5306-7597> (accessed on 5 January 2023).

14. Honaker, R.; Groppo, J.; Yoon, R.-H.; Luttrell, G.; Noble, A.; Herbst, J. Process evaluation and flowsheet development for the recovery of rare earth elements from coal and associated byproducts. *Miner. Metall. Process.* **2017**, *34*, 107–115. [[CrossRef](#)]
15. Honaker, R.; Zhang, W.; Werner, J. Acid leaching of rare earth elements from coal and coal ash: Implications for using fluidized bed combustion to assist in the recovery of critical materials. *Energy Fuels* **2019**, *33*, 5971–5980. [[CrossRef](#)]
16. Zhang, W.; Honaker, R. Calcination pretreatment effects on acid leaching characteristics of rare earth elements from middlings and coarse refuse material associated with a bituminous coal source. *Fuel* **2019**, *249*, 130–145. [[CrossRef](#)]
17. Zhang, W.; Honaker, R. Characterization and recovery of rare earth elements and other critical metals (Co, Cr, Li, Mn, Sr, and V) from the calcination products of a coal refuse sample. *Fuel* **2020**, *267*, 117236. [[CrossRef](#)]
18. Ji, B.; Li, Q.; Zhang, W. Leaching Recovery of Rare Earth Elements from Calcination Product of a Coal Coarse Refuse Using Organic Acids. *J. Rare Earths* **2020**, *40*, 318–327. [[CrossRef](#)]
19. Zhang, W.; Noble, A.; Ji, B.; Li, Q. Effects of contaminant metal ions on precipitation recovery of rare earth elements using oxalic acid. *J. Rare Earths* **2020**, *40*, 482–490. [[CrossRef](#)]
20. Cheremisina, O.; Sergeev, V.; Fedorov, A.; Alferova, D.; Lukyantseva, E. Study of iron stripping from DEHPA solutions during the process of rare earth metals extraction from phosphoric acid. *ARPN J. Eng. Appl. Sci.* **2019**, *8*, 1591–5.
21. Li, Q.; Ji, B.; Honaker, R.; Noble, A.; Zhang, W. Partitioning behavior and mechanisms of rare earth elements during precipitation in acid mine drainage. *Colloids Surf. A Physicochem. Eng. Asp.* **2022**, *641*, 128563. [[CrossRef](#)]
22. Nawab, A.; Yang, X.; Honaker, R. Parametric study and speciation analysis of rare earth precipitation using oxalic acid in a chloride solution system. *Miner. Eng.* **2022**, *176*, 107352. [[CrossRef](#)]
23. Lauf, R.J.; Harris, L.A.; Rawlston, S.S. Pyrite framboids as the source of magnetite spheres in fly ash. *Environ. Sci. Technol.* **1982**, *16*, 218–220. [[CrossRef](#)]
24. Schweinfurth, S.P.; Finkelman, R.B. Coal—A complex natural resource: An overview of factors affecting coal quality and use in the United States. *Report* **1143**, 2002.
25. Finkelman, R.B. Modes of occurrence of potentially hazardous elements in coal: Levels of confidence. *Fuel Process. Technol.* **1994**, *39*, 21–34. [[CrossRef](#)]
26. Wang, L.; Pan, Y.; Li, J.; Qin, H. Magnetic properties related to thermal treatment of pyrite. *Sci. China Ser. D: Earth Sci.* **2008**, *51*, 1144–1153. [[CrossRef](#)]
27. Hu, G.; Dam-Johansen, K.; Wedel, S.; Hansen, J.P. Decomposition and oxidation of pyrite. *Prog. Energy Combust. Sci.* **2006**, *32*, 295–314. [[CrossRef](#)]
28. Moldoveanu, G.A.; Papangelakis, V.G. Recovery of rare earth elements adsorbed on clay minerals: I. Desorption mechanism. *Hydrometallurgy* **2012**, *117*, 71–78. [[CrossRef](#)]
29. Honaker, R.; Zhang, W.; Werner, J.; Noble, A.; Luttrell, G.; Yoon, R. Enhancement of a process flowsheet for recovering and concentrating critical materials from bituminous coal sources. *Min. Metall. Explor.* **2020**, *37*, 3–20. [[CrossRef](#)]
30. Valian, A. Characterization of Rare Earth Elements in the Illinois Basin Coals. Ph.D. Thesis, University of Kentucky, Lexington, KY, USA, 2020. Available online: <https://orcid.org/0000-0002-7289-4213> (accessed on 18 December 2022).
31. Karunadasa, K.S.P.; Manoratne, C.H.; Pitawala, H.M.T.G.A.; Rajapakse, R.M.G. Thermal decomposition of calcium carbonate (calcite polymorph) as examined by in-situ high-temperature X-ray powder diffraction. *J. Phys. Chem. Solids* **2019**, *134*, 21–28. [[CrossRef](#)]
32. Zhang, W.; Honaker, R.Q. Rare earth elements recovery using staged precipitation from a leachate generated from coarse coal refuse. *Int. J. Coal Geol.* **2018**, *195*, 189–199. [[CrossRef](#)]

**Disclaimer/Publisher’s Note:** The statements, opinions and data contained in all publications are solely those of the individual author(s) and contributor(s) and not of MDPI and/or the editor(s). MDPI and/or the editor(s) disclaim responsibility for any injury to people or property resulting from any ideas, methods, instructions or products referred to in the content.